Towards a 3-D finite element model for the gas-assisted injection moulding process

G. A. A. V. Haagh, H. Zuidema, F. N. van de Vosse, G. W. M. Peters and H. E. H. Meijer*

Centre for Polymer and Composites, Eindhoven University of Technology, Eindhoven, The Netherlands

Towards a 3-D Finite Element Model for the Gas-Assisted Injection Moulding Process

The Gas-Assisted Injection Moulding process (GAIM) offers a number of advantages, which are almost without exception related to the negligible pressure drop in the gas core of the moulded product. Accurate prediction of the gas distribution inside GAIM products is, however, still a major problem to be solved. As gas penetration is governed by three-dimensional phenomena, one has to resort to numerical simulations to analyse the process. Therefore, a numerical model for GAIM simulations has been developed, based on a physical, rather than on an empirical approach. The model employs a pseudo-concentration method in order to avoid elaborate three-dimensional remeshing, and has been implemented in a finite element program.

Simulation results for two-dimensional test cases representing typical GAIM situations prove that the model covers most of the important aspects of gas injection. A pilot simulation for a simple three-dimensional mould demonstrates that the model is able to deal with three-dimensional GAIM. Further refinement of the model will mainly concern the implementation of faster and less memory-consuming solution methods.

1 Introduction

In Gas-Assisted Injection Moulding (GAIM), gas is injected into a mould that has been filled partially with polymer. The gas drives the molten polymer core further into the mould until it is filled completely, thus yielding a product with a polymer skin and a hollow core. The gas is then used to transmit the packing pressure to the polymer skin and the polymer shrinkage is compensated for by an enlargement of the gas core. Once the polymer skin has been solidified completely, the gas pressure is released.

A major characteristic of GAIM is that the pressure gradient in the gas core is negligibly small compared to the pressure gradient in the polymer melt, due to the large polymer/gas viscosity ratio, which is of the order of 10^8. As a result, the pressure in the gas core can be considered constant. The gas penetrates in the direction of the largest pressure gradient (often called the path of least flow resistance), which is typically found in the thicker parts of the mould, such as ribs or specially designed gas leading channels. As soon as the gas enters a thin-walled section, the gas front will become unstable – the so-called finger-effect– and the process stability becomes difficult to control.

The negligible pressure gradient in the gas core is the basis for most of the advantages of the GAIM process. First of all, it leads to a reduction in the moulding pressure (Fig. 1). Moreover, the pressure is distributed more uniformly over the mould, since the gas pressure is constant throughout the gas core. This is a potential way to reduce residual stresses and warpage. The presence of the gas core in thick-walled parts will also reduce the occurrence of sink marks. Furthermore, cooling times may be decreased, yielding shorter cycle times. And, finally, GAIM allows for (partially) thick-walled products that were to be avoided in conventional injection moulding; therefore it enhances the product design possibilities.

On the other hand, the characteristics of GAIM complicate the control of the process. Because the direction of the largest pressure gradient along which the gas front proceeds is unique, splitting of the gas flow usually leads to uncontrolled gas penetration [1]. Any minor disturbance in the pressure gradient in one of the branches of a bifurcation will cause one of the gas fronts to run ahead and the other one to stop.

The flow field at the gas front determines the polymer skin thickness that remains after the gas front has passed [2]. This skin thickness, together with the gas penetration length, is very important, as it yields information about the ratio of polymer and gas to be injected. In the GAIM process, the gas injection stage is often considered analogous to two-component injection moulding. There is, however, an important difference, which is shown in Fig. 2. In co-injection moulding – where both components have viscosities of the same order – the velocity profile at the interface is (quasi-)parabolic in both materials, implying

* Mail address: G. A. A. V. Haagh, Centre for Polymers and Composites, Eindhoven University of Technology, P.O. Box 513, 5600 MB Eindhoven, The Netherlands

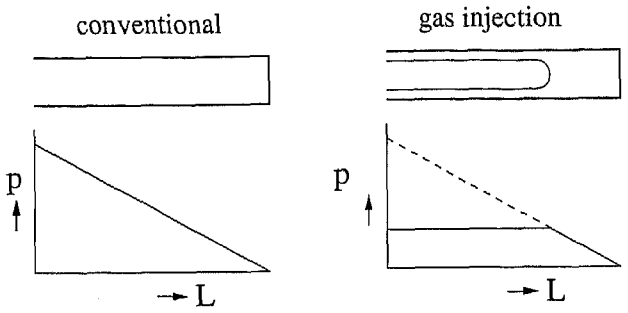

Fig. 1. Pressure distribution in GAIM compared to conventional injection moulding

that velocities in the thickness direction can be neglected. In GAIM, the pressure at the gas front induces velocities that have a significant component in the thickness direction. Moreover, the gas penetrates through thick-walled parts, which are essentially three-dimensional geometries.

From a physical perspective, GAIM is similar to expelling a viscous fluid from a tube with a less viscous fluid. In this context, Taylor [3] did an experimental study on the isothermal penetration of water into a highly viscous fluid in a horizontal axisymmetric tube. He found that the residual wall thickness of the viscous fluid was determined by the Capillary number Ca, which is the ratio of viscous and interfacial forces defined as

$$\mathrm{Ca} = \frac{\eta U}{\gamma}, \tag{1}$$

in which η is the viscosity of the highly viscous fluid, U is the characteristic velocity, and γ is the interfacial tension. For increasing Capillary numbers, the residual wall thickness increased towards an asymptotical value of 34 % of the tube radius.

Poslinski et al. [2, 4] carried out both an experimental and a numerical analysis of isothermal gas penetration into a Power-Law fluid. At high Capillary numbers – which is usually the case in GAIM – they found a relative wall thickness of 0.37 for a Newtonian fluid, which however decreased with decreasing Power-Law exponent (Fig. 3). They justify their isothermal approach as useful for GAIM analysis by showing that the gas penetration time is much smaller that the typical solidification time for the polymer.

In spite of these and other studies, it has not been possible to derive a generally applicable (analytical) expression for gas penetration into a viscous fluid. Therefore, we have to resort to a numerical model of the process. In this paper, we will develop such a model in order to gain understanding of the gas distribution in a GAIM product. Fig. 4 gives some typical examples of gas distributions that one wants to predict. Since gas injection is governed by three-dimensional phenomena, as we have explained above, the Hele-Shaw or thin-film approximation that is commonly adopted for the modelling of injection moulding of thin-walled products, is not applicable to GAIM.

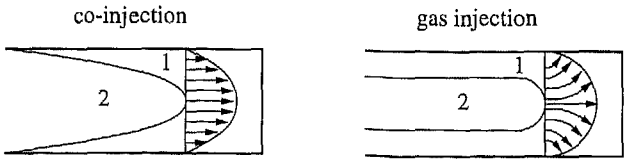

Fig. 2. Velocity distribution in GAIM compared to co-injection moulding

In recent years, a few research groups have recognised the need for three-dimensional simulation of the GAIM process, and started developing simulation codes. Costa et al. [5] employed the boundary element method, starting with a non-isothermal problem of gas injection into a generalised Newtonian fluid between two parallel plates as a two-dimensional test problem. The polymer front and the gas front were both treated as moving boundaries of the computational domain. Khayat et al. [6] used a similar approach to model isothermal gas injection into an incompressible, Newtonian fluid in a simple three-dimensional geometry. These simulations did not resolve many details, since they could only be done using a coarse mesh, due to CPU and storage problems. Both papers show qualitative results that appear to agree with practical GAIM experience, but no quantitative results are given. Also, in the existing simulation codes for injection moulding, sometimes a gas-injection option becomes available. The usefulness thereof is questionable, however, since all these codes are essentially based on the so-called $2\frac{1}{2}$D approach, applying the Hele-Shaw or thin-film approximation [7, 8].

In order to do useful GAIM simulations, any model should be able to deal with gas injection in three-dimensional geometries, since the practical questions to be answered are principally 3D. Furthermore, a model should be based on a physical approach to the problem, and approximation formulae as they have appeared in the literature [2, 9] are to be avoided.

The aim of this paper is to present the principles of a numerical model that fulfils those requirements and to demonstrate its capabilities. Therefore, no sophisticated simulations of real GAIM processes will be shown and we will limit ourselves to isothermal flow of incompressible, Newtonian fluids. The model itself is presented in section 2, and its implementation in a finite element code is treated in section 3. In section 4 a number of simulation results will be discussed, leading to conclusions given in section 5.

2 Modelling

2.1 Method

The model presented is based on a pseudo-concentration method [10]. With this method, the flow problem is solved on a fixed grid that covers the entire mould, and elaborate three-dimensional remeshing is avoided. A fictitious fluid is introduced to represent both the air downstream of the polymer flow front and the injected gas. The main property of this fictitious fluid is that it should not contribute to the pressure build-up in the mould during filling. Therefore, its viscosity is set to a value at least 10^3 times smaller than the viscosity of the filling fluid. However, the viscosity of the fictitious fluid exceeds the real value for air by several orders of magnitude in order to keep the Reynolds number

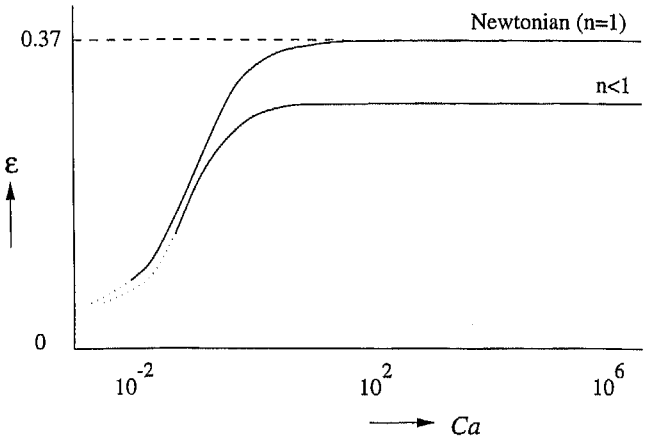

Fig. 3. Residual wall thickness as a function of the Capillary number for Newtonian and Power-Law fluids ($\eta = \eta_0 \dot{\gamma}^{n-1}$). (After [4].)

small (see the next section). Furthermore, the fictitious fluid is allowed to leave the mould at selected places.

The distinction between the polymer and the fictitious fluid is made by labelling fluid particles with a material label c (being the 'pseudo-concentration'), which is given the value c = 1 for the polymer, and c = 0 for the fictitious fluid. Near the polymer front and the gas front, c is a continuous function between 0 and 1; the interfaces themselves are determined by the iso-value lines for c = 0.5. The interfaces are kept track of by convecting the material labels with the fluid velocity (Fig. 5).

A comparable approach is used by Chen et al. [11]. However, as they use the Hele-Shaw approximation – thus neglecting the velocity components in thickness direction – they have to estimate the residual wall thickness beforehand. In the method given here, no such a priori assumption is made whatsoever.

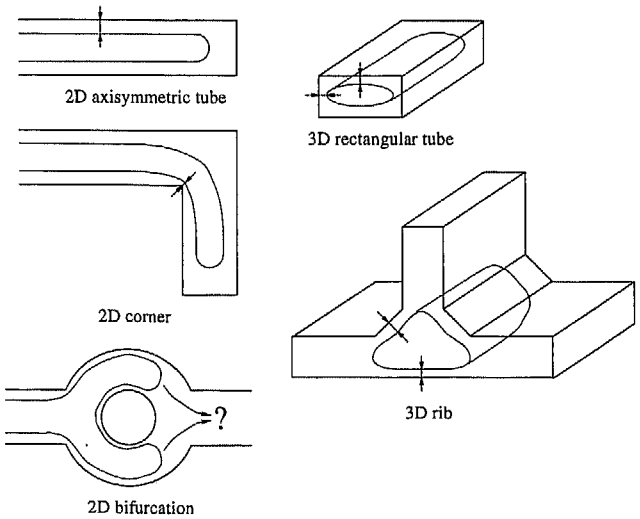

Fig. 4. Typical examples of gas distributions in GAIM products

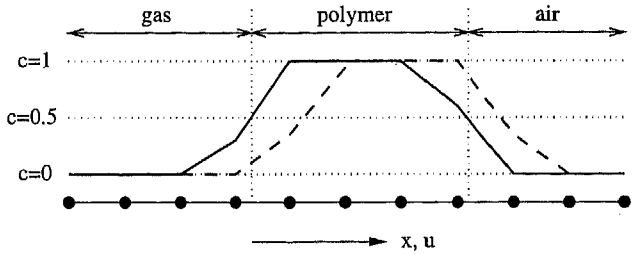

Fig. 5. Convection of the material labels: —— time step n, --- time step n + 1

2.2 Governing Equations

As mentioned, the flow is considered incompressible and isothermal, thus the conservation equations for mass and momentum reduce to the Navier-Stokes equations

$$\vec{\nabla} \cdot \vec{u} = 0, \tag{2}$$

$$\varrho \frac{\partial \vec{u}}{\partial t} + \varrho \vec{u} \cdot \vec{\nabla} \vec{u} = \vec{\nabla} \cdot \sigma + \varrho \vec{g}. \tag{3}$$

The constitutive equation for the Cauchy stress tensor $\boldsymbol{\sigma}$ is given by:

$$\boldsymbol{\sigma} = -\varrho \mathbf{I} + \boldsymbol{\sigma}^d, \tag{4}$$

$$p = p_0 - \mu \, \mathrm{tr}\,(\mathbf{D}), \tag{5}$$

$$\boldsymbol{\sigma}^d = 2\eta \mathbf{D}^d, \tag{6}$$

in which generalised Newtonian behaviour is assumed for the viscosity

$$\eta = \eta(p, \mathbf{D}^d). \tag{7}$$

Each variable in Eqs. (2) to (7) can be written as a product of a dimensionless variable and its characteristic value (Table 1). The ratio ε determines the type of mould geometry. Since the gas is usually led through gas channels or ribs, we can limit ourselves to oblong geometries ($\varepsilon < 1$).

The conservation equations can now be expressed in their dimensionless form; when normalising all terms in the equation of conservation of momentum with respect to the stationary inertia forces, this yields

$$\vec{\nabla} \cdot \vec{u} = 0, \tag{8}$$

$$\mathrm{Sr} \frac{\partial \vec{u}}{\partial t} + \vec{u} \cdot \vec{\nabla} \vec{u} = -\frac{1}{\mathrm{Re}} \vec{\nabla} p + \frac{1}{\mathrm{Re}} \vec{\nabla}(2\mathbf{D}^d) + \frac{1}{\mathrm{Fr}} \vec{g}, \tag{9}$$

*Table 1. Process variables expressed as products of dimensionless variables (marked with a *) and characteristic values*

$x = x^* L$	$y = y^* H = y^* \varepsilon L$	$z = z^* H = z^* \varepsilon L$
$u = u^* U$	$v = v^* V = v^* \varepsilon U$	$w = w^* V = w^* \varepsilon U$
$\nabla_x = \nabla_x^* \frac{1}{L}$	$\nabla_y = \nabla_y^* \frac{1}{H} = \nabla_y^* \frac{1}{\varepsilon L}$	$\nabla_z = \nabla_z^* \frac{1}{H} = \nabla_z^* \frac{1}{\varepsilon L}$
$\varepsilon = \frac{H}{L}$	$t = t^* \tau$	
$p = p^* \frac{\eta U}{H}$	$\mathbf{D}^d = \mathbf{D}^{d*} \frac{U}{H}$	$\vec{g} = \vec{g}^* g_0$

from which the * indicating dimensionless variables have been removed. The dimensionless numbers are given by

$$\mathrm{Re} = \frac{\varrho UH}{\eta} \quad \mathrm{Sr} = \frac{L}{\tau U} \quad \mathrm{Fr} = \frac{U^2}{g_0 L}. \tag{10}$$

Characteristic values for polymer injection are given in Table 2. The characteristic time τ is the time scale upon which velocity fluctuations of order U occur. In injection moulding, such a fluctuation will only occur immediately after starting the process. As we are not interested in start-up phenomena, τ is very large with respect to $\frac{L}{U}$, and consequently the Strouhal number Sr is very small. The other dimensionless numbers can be determined as:

$$\mathrm{Re} = \begin{cases} 10^{-3} \text{ for polymer} \\ 10^{2} \text{ for air and gas} \end{cases}$$

$$\mathrm{Fr} = 10^{-2} \tag{11}$$

For the polymer domain, the Reynolds number indicates that the stationary inertia terms can be neglected with respect to the viscous stress term, resulting in a linear Stokes equation. (Inertia forces may become important in pressure-controlled GAIM at the end of the gas injection stage, when the polymer front is strongly accelerated; this is not considered in this paper). However, for the air and gas domains the stationary inertial forces cannot be neglected, which leaves the (non-linear) Navier-Stokes equations to be solved. To avoid this, the air and the gas are replaced by a fictitious fluid, of which the viscosity is of order 10^{-3} of the polymer viscosity, and which has the same density as air. Consequently, the Reynolds number for the fictitious fluid domains reduces to $\mathrm{Re} = 10^{-3}$, while the pressure drop is still negligibly small compared to the pressure drop in the polymer domain. As a result, the flow problem is described by a stationary Stokes equation for the entire computational domain

$$\vec{\nabla} p = \vec{\nabla}(2\mathbf{D}^{d}) + \frac{\mathrm{Re}}{\mathrm{Fr}} \vec{g}. \tag{12}$$

As the ratio of gravitational and viscous forces, given by the ratio of Reynolds number and Froude number $\frac{\mathrm{Re}}{\mathrm{Fr}}$, is of the order 10^{-1}, the gravitational forces can be neglected as well.

The material labels that are used to distinguish polymer from air, are convected through the mould with velocity $\vec{u}$. Thus, a pure (passive scalar) convection equation describes the evolution of the material label distribution

Table 2. Characteristics values of the process variables for polymer injection moulding

Variable	Unit	Characteristic value Polymer	Air/gas
ϱ	kg m^{-3}	10^3	1
η	Pa s	10^3	10^{-5}
L	m	10^{-1}	
H	m	10^{-2}	
τ	s	10^{-1}	
U	m s^{-1}	10^{-1}	
g_0	m s^{-2}	10	
γ	N m^{-1}	10^{-2}	

$$\dot{c} = \frac{\partial c}{\partial t} + \vec{u} \cdot \vec{\nabla} c = 0. \tag{13}$$

Actually, this can be regarded as a conservation equation of particle identity.

The mould filling problem can thus be simulated by solving Eqs. (12) and (13) and updating the material properties at every time step.

2.3 Boundary Conditions

We define a domain Ω covering the mould, with boundaries Γ_e, Γ_w, and Γ_v designating the mould entrance, the mould walls and the air vents respectively. At the mould entrance, either the injection flow rate or the injection pressure is prescribed. Wherever the mould wall is covered with polymer, a no-slip condition is imposed. The physically correct boundary conditions near the moving contact line, however, cannot be uniquely determined, since the physics of this phenomenon are still not completely understood [12]. As a no-slip boundary condition in the air would prevent the polymer from contacting the mould wall, we have chosen to prescribe a free slip condition downstream of the flow front, thus enabling the contact point to move freely and preventing the polymer to leave the computational domain. Hence, the boundary condition at the mould walls is a function of the type of material. This has been implemented by using an adjustable Robin boundary condition for the velocity components u_t in tangential direction

$$a u_t + \frac{\partial u_t}{\partial x_t} = 0 \quad \forall \vec{x} \in \Gamma_w, \forall \vec{x} \in \Gamma_v, \tag{14}$$

in which

$$a = a(c) = \begin{cases} 10^9 \text{ if } c \geq 0.5 \\ 0 \text{ if } c < 0.5 \end{cases}. \tag{15}$$

The mould walls are impermeable, except at the air vents Γ_v where the air is allowed to leave the mould, yielding the following boundary condition for the velocity component u_n in normal direction:

$$u_n = 0 \quad \forall \vec{x} \in \Gamma_w \tag{16}$$

$$a u_n + \frac{\partial u_n}{\partial x_n} = \quad \forall \vec{x} \in \Gamma_v \tag{17}$$

in which a and b are again given by Eq. (15).

2.4 Interfacial Conditions

From a physical point of view, two more boundary conditions hold for the flow front and the gas front, namely immiscibility and conservation of momentum. The immiscibility condition is already implied by the 'conservation of identity' Eq. (13). The conservation of momentum at an interface is expressed as [13]

$$(\boldsymbol{\sigma}_2 - \boldsymbol{\sigma}_1) \cdot \vec{n}_{12} = \gamma_{12} \kappa \vec{n}_{12}, \tag{18}$$

whereas the subscripts 1 and 2 denote the polymer and the fictitious fluid, and γ_{12}, κ, and $\vec{n}_{12}$ denote the interfacial tension, the interface curvature and the normal vector to

the interface respectively. Using Eq. (6) and introducing dimensionless variables, Eq. (18) can be written as:

$$(\boldsymbol{\sigma}_2 - \boldsymbol{\sigma}_1) \cdot \vec{n}_{12} = \frac{1}{Ca} \kappa \gamma_{12} \vec{n}_{12}. \tag{19}$$

For GAIM, the Capillary number is of order 10^3, indicating that interfacial forces can be neglected. Thus Eq. (18) is reduced to

$$\boldsymbol{\sigma}_2 - \boldsymbol{\sigma}_1 = \mathbf{0}, \tag{20}$$

which is already taken care of by the 'overall' conservation of momentum equation Eq. (9), since the material properties are continuous functions of c at the interface. As a result, the phenomena at the flow front have already been taken into account in our model.

3 Numerical Methods

The model has been implemented in the finite element package SEPRAN [14]. This section gives a short description of the implementation.

3.1 The Stokes Equation

The continuity equation and the Stokes equation are solved using the penalty function method, in which the continuity equation is replaced by [15]

$$\frac{1}{\lambda} p + \vec{\nabla} \cdot \vec{u} = 0. \tag{21}$$

If the penalty parameter λ is very large, the continuity equation is still satisfied. After spatial discretisation using a standard Galerkin finite element method, the resulting equations can be written as

$$S\underline{u} + L^T\underline{p} = \underline{f}, \tag{22}$$

$$D\underline{p} = \lambda L\underline{u}, \tag{23}$$

in which $\underline{f}$ is the right hand side vector containing the essential boundary conditions, and

$$S_{ij} = \frac{1}{Re} \int_\Omega \vec{\nabla}\phi_i \cdot \vec{\nabla}\phi_j \, d\Omega,$$

$$L_{ij} = -\int \psi_i \vec{\nabla}\phi_j \, d\Omega,$$

$$D_{ij} = \int_\Omega \psi_i \psi_j \, d\Omega,$$

and ϕ_i and ψ_i are the shape functions for the velocity and the pressure respectively.

Substitution of Eq. (22) in Eq. (23) yields

$$S\underline{u} + \lambda L^T D^{-1} L\underline{u} = \underline{f}. \tag{24}$$

This equation is solved with a direct solver using quadratic rectangular elements for two-dimensional meshes and 27-node brick elements for three-dimensional meshes [14]; the pressure can be calculated afterwards from Eq. (23).

The material parameters are defined as discontinuous functions of the material labels, i.e.:

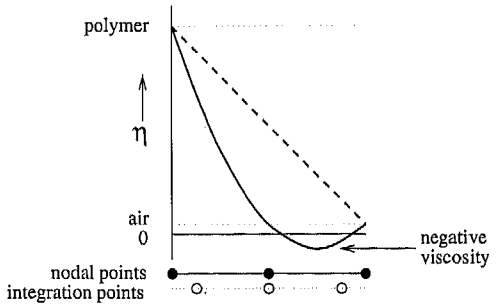

Fig. 6. Linear interpolation of the viscosity on a quadratic element: —— original function, – – – interpolated function

$$\eta = \eta(c) = \begin{cases} \eta_{polymer} & \text{if } c \geq 0.5 \\ \eta_{fictitious} & \text{if } c < 0.5 \end{cases} \tag{25}$$

The use of quadratic shape functions may then lead to numerical problems, e.g. negative viscosities at the elements' integration points (Fig. 6). This is avoided by linear interpolation of the material parameter at the midpoints of elements containing the flow front [16].

3.2 The Convention Equation

The pure convection equation for the material labels is solved with the finite element method using an SUPG scheme incorporating Shakib's parameter suggested for time-dependent problems [17]. Only one boundary condition (at the flow entrance) is needed

$$c = \begin{cases} 1 \text{ if } t < t_{gas} \\ 0 \text{ if } t \geq t_{gas} \end{cases} \quad \forall \vec{x} \in \Gamma_e, \tag{26}$$

where t_{gas} is the time at which gas is injected. Initially, c is set to zero in the entire domain Ω.

Applying spatial discretisation, the convection equation can be written in the form

$$M\underline{c} + N(\underline{u})\underline{c} = 0, \tag{27}$$

in which M is the mass matrix and $N(\underline{u})$ is the stiffness matrix. Temporal discretisation with a finite difference θ-method yields

$$M\frac{\underline{c}^{n+1} - \underline{c}^n}{\Delta t} + \theta N(\underline{u}^{n+1})\underline{c}^{n+1} + (1-\theta)N(\underline{u}^n)\underline{c}^n = 0, \tag{28}$$

in which the superscripts $n+1$ and n indicate consecutive time steps. This can be rewritten into a two-step procedure

$$\frac{M}{\theta\Delta t}\underline{c}^{n+\theta} + N(\underline{u}^{n+\theta})\underline{c}^{n+\theta} = \frac{M}{\theta\Delta t}\underline{c}^n, \tag{29}$$

$$\underline{c}^{n+1} = \frac{1}{\theta}(\underline{c}^{n+\theta} - (1-\theta)\underline{c}^n). \tag{30}$$

For the time discretisation, a modified version of the Crank-Nicolson scheme ($\theta = 0.5$) is used: θ is set to $0.5 + \alpha\Delta t^*$, in which Δt^* is the dimensionless time step given by $\Delta t^* = \frac{\Delta t}{t_{end} - t_0}$ and α is a small positive real number. This modification of θ suppresses oscillations without affecting the order of accuracy. The material labels are rounded off to either unity or zero everywhere, except in the elements

containing the flow front, where the original values of the material labels are retained. Hence, oscillations in the material label field are suppressed, and the flow front is tracked quite accurately.

4 Results and Discussion

In order to show that the model described in this paper captures the important aspects of the GAIM process, some two-dimensional cases as well as a three-dimensional case are presented. First, we consider gas injection in an axisymmetric cylinder, which enables us to compare the results with experimental results that have appeared in the literature. Next, two cases are shown that exhibit typical GAIM phenomena: gas injection around a sharp corner, and gas injection in a bifurcation. Finally, it is demonstrated that the model is able to deal with GAIM in three-dimensional moulds.

4.1 Axisymmetric Cylinder

As an initial test for the model, we have simulated the GAIM process of an axisymmetric cylinder, for which results are available in the literature [2, 3]. The test geometry and the parameters are given in Fig. 7 and Table 3. A parabolic velocity profile is prescribed at the flow entrance Γ_e; the polymer is injected over the entire radius, whereas the gas is injected over 40 % of the radius at the same flow rate. An air vent has been defined at Γ_v.

Each particle entering the mould has not only been labelled with its material label c, but also with its injection time. The colours in Fig. 8(a) to 8(e) represent these injection time labels at five stages of the process: the alternating yellow and black colours visualise the development of fountain flow at the polymer front, whereas air and injected gas are represented by light and dark blue respectively. Because of time discretisation errors, the dark blue colour covers the entire injection boundary. The anomaly in the time label distribution at the lower right corner (Fig. 8(d) and 8(e)) is an artifact of the time label convection; it is absent in the material label distribution (Fig. 8(f)).

If the gas is injected too early, the gas will break through the polymer front. Fig. 8(g) shows that our model is capable of predicting breakthrough.

The relative polymer skin thickness resulting from this simulation is 33 % of the tube radius, which agrees well with the experimental and analytical results from the literature that were mentioned in the introduction. Table 4 shows that at least 10 elements were needed in the radial direction for the skin thickness to converge to this value. In the axial direction, at least 20 elements were required for an accurate representation of the moving polymer front. The polymer volume loss due to the pseudo-concentration method – which is directly related to the accuracy of the determination of the gas and polymer fronts – is within 2 %.

Table 3. Process parameters for the GAIM simulations

Mould type	Axisymmetric cylinder	Sharp corner	3-D box
Dimensions	L = 100 mm R = 5.0 mm	L = 110 mm H = 10 mm	L = 100 mm $\frac{1}{2}$W = 15 mm $\frac{1}{2}$H = 5 mm
Viscosity ratio	10^3	10^3	10^3
Filling time	1.0 s	2.1 s	1.0 s
Gas injection time	0.57 s	0.9 s	0.5 s
# elements	200	1 009	480
# time steps	100	210	100

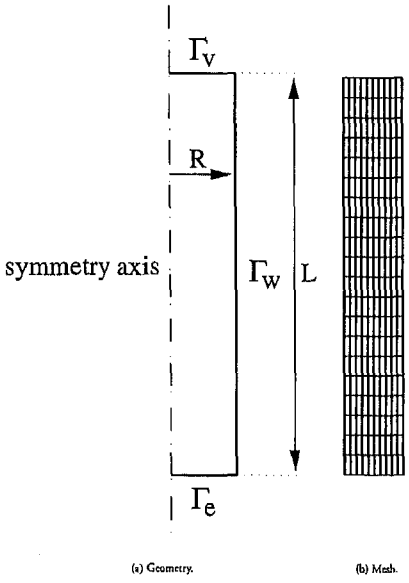

Fig. 7. Computational domain for the axisymmetric cylinder

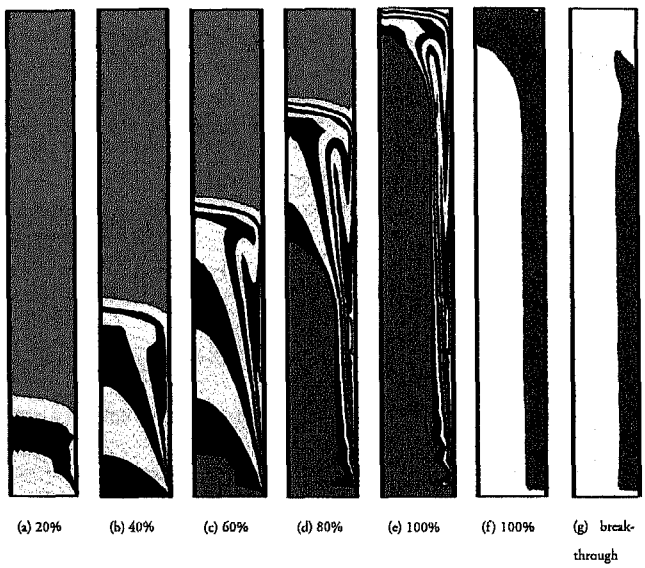

Fig. 8. Simulation results for an axisymmetric tube at several filling stages; (a)–(e): injection time labels (light blue = air, yellow and black = polymer, dark blue = gas); (f)–(g); material labels (gray = polymer, white = fictitious fluid). In (g) gas breakthrough was enforced by injecting gas already after 0.45 s. Note that these plots are extended in radial direction

Table 4. Polymer volume percentage and polymer skin fractions for different meshes. Theoretical polymer volume percentage is 57 % for $t \geq t_{gas}$. (L and R as defined in Figure 7; δ = polymer skin thickness as fraction of cylinder radius; m = polymer skin cross-sectional area as fraction of cylinder cross-section.)

Elements L × R	Δt	Vol % polymer at t_{gas}	Vol % polymer at t_{end}	δ	m
10 × 5	0.02	54.73	55.32	0.30	0.51
20 × 10	0.01	56.77	57.57	0.32	0.54
40 × 20	0.005	56.85	58.00	0.33	0.55

4.2 Gas Flow around a Sharp Corner

From common GAIM experience, it has become clear that sharp corners in gas leading channels are to be avoided: the polymer skin usually becomes very thin at the inner corner, and the gas may even break through the skin. This is inherent to the nature of the gas flow, which advances in the direction of largest pressure gradient. Fig. 9 and Table 3 give the geometry and the parameters for a two-dimensional simulation of gas flow around a sharp corner. Note that an extra air vent at the corner had to be defined in order to avoid air entrapment.

From the simulation results (Fig. 10) it can be concluded that the model is able to predict the advancement of both the polymer and the gas front around a sharp corner. The symmetrical shape of the polymer front, which is disturbed by the corner (Fig. 10(b)), is restored after some time. The final gas distribution clearly shows that the gas front has taken a 'short-cut' around the corner, after which it has returned to the centre of the channel (Fig. 10(e)). This indicates that the cross-sectional gas distribution eventually becomes insensitive to the gas injection location.

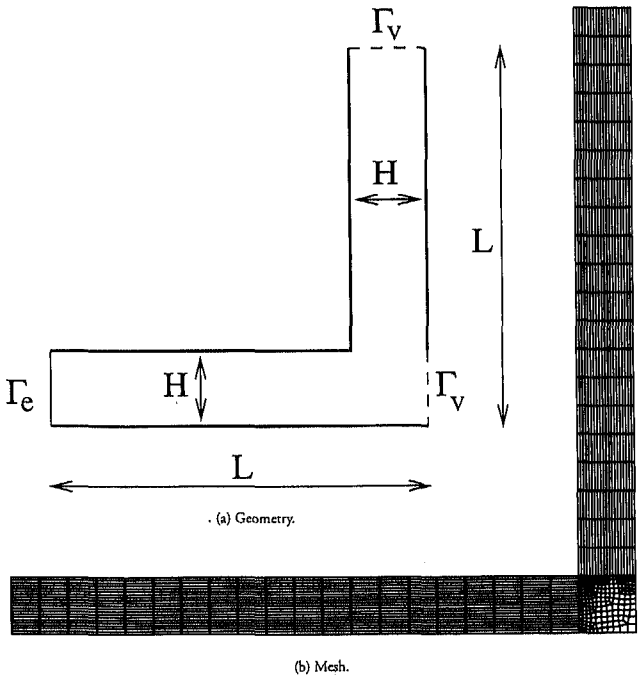

Fig. 9. Computational domain for the axisymmetric cylinder

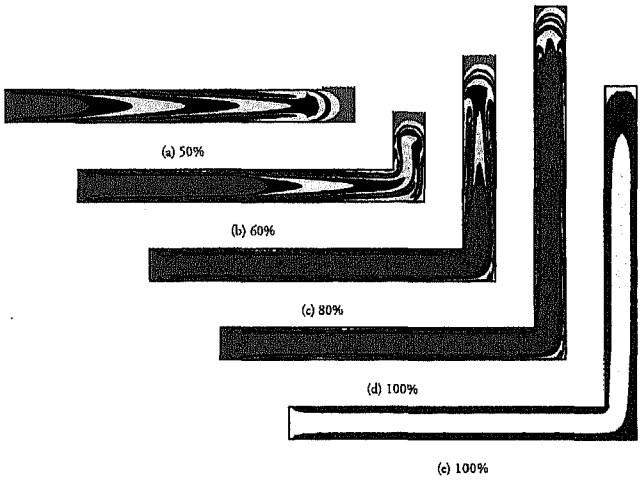

Fig. 10. Simulation results for 2D gas flow around a sharp corner; (a)–(d): injection time labels (light blue = air, yellow and black = polymer, dark blue = gas); (e): material labels (gray = polymer, white = fictitious fluid)

4.3 Bifurcation of the Gas Flow

As explained in the introduction, a bifurcation of the gas flow will lead to an asymmetric gas core, even if the mould is symmetric. To test whether our model is able to deal with this phenomenon, an example of a bifurcation was taken from the IKV videotape on GAIM [18] (see Fig. 11). To introduce a slight disturbance, the cross-section at the end of the right branch of the ring was made 2.5 % smaller than at the left branch. Initially, the mould was completely filled with polymer, and only the gas injection stage was simulated. Both polymer and gas could leave the mould freely at the exit on the top.

To simulate the asymmetric gas penetration in full detail, a very fine mesh and small time steps are needed, since the stopping and the proceeding gas channels are separated

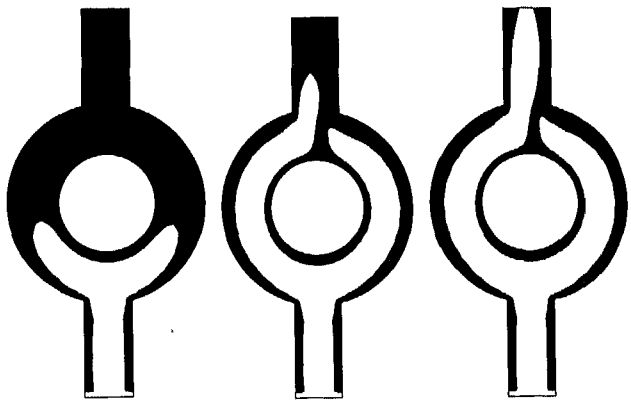

Fig. 11. Development of the gas channel in a flow bifurcation; material labels (gray = polymer, white = fictitious fluid)

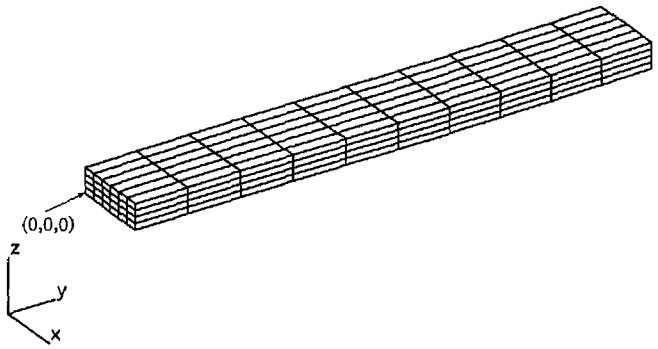

Fig. 12. Mesh for the three-dimensional rectangular tube

only by a thin 'dam' of polymer that arises over a very short period of time. However, as our aim here is to demonstrate this effect rather than perform detailed simulations, we have used a relatively coarse mesh and large time step. Consequently, the viscosity ratio of polymer and gas had to be set to 10^4 to be able to obtain the asymmetric gas distribution shown in Fig. 11. It can be seen that after an initially symmetrical gas penetration, the slightly lower flow resistance in the left branch causes the left gas front to run ahead, while the right gas front ultimately stops. In a qualitative sense, these results compare well to the observations recorded on the IKV videotape.

4.4 Three-Dimensional Rectangular Tube

Since GAIM is governed by three-dimensional phenomena, our ultimate aim is to perform simulations on three-dimensional moulds. However, the combination of a penalty method and a direct solver for the Stokes equation is inefficient with respect to computing time and memory usage. This is a limitation of the solution method, rather than of the model itself. This problem will be solved in the future by the use of an iterative solver. We would like to remark that full three-dimensional remeshing – which is avoided with our method – demands for even larger computing times.

The three-dimensional mould presented here is a rectangular tube, which has two planes of symmetry: $x = 0$ and $z = 0$ (Fig. 12 and Table 3). Therefore, only one quarter has to be modelled. This mesh is relatively coarse in order to keep computing times within reasonable limits (approximately two days on a Silicon Graphics Power Challenge). Although no quantitative results are available in the literature for comparison, the predicted polymer and gas flow fronts seem to be quite realistic (Fig. 13). The coarseness of the mesh, together with the large gradients in the injection time labels near the mould walls, causes some numerical oscillations in the time label field. Therefore, the fountain flow effect cannot be visualised. Because such large gradients are absent in the material label field, the polymer and gas flow front do not suffer from oscillations.

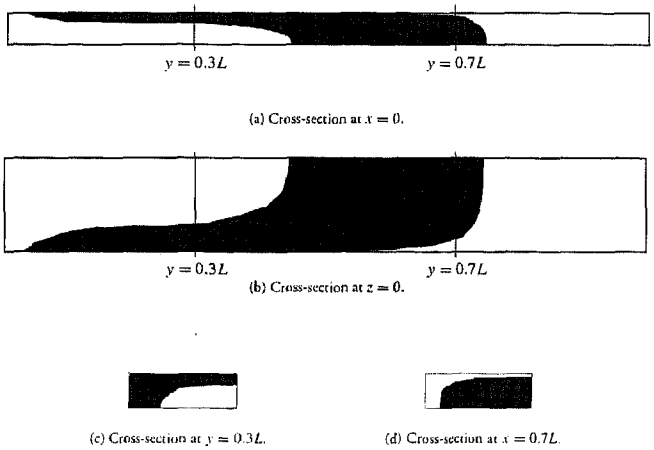

Fig. 13. Simulation results for the three-dimensional rectangular tube; material labels (gray = polymer, white = fictitious fluid)

5 Conclusions

The major question to be solved in GAIM processes is the gas distribution inside the product. As the gas penetration is essentially a three-dimensional process – due to the nature of the gas flow and the geometrical conditions – , a numerical model for GAIM should be able to perform three-dimensional simulations.

Such a model, adopting a pseudo-concentration method, has been developed. It is based on the physical characteristics of the process, rather than on empirical approximations of the gas distribution. As a result, some (isothermal) test cases have proven that the model covers the important aspects of GAIM: the residual polymer skin thickness is predicted accurately, and typical GAIM phenomena such as a decreased skin thickness at the inner side of a sharp corner, and asymmetric gas penetration in a bifurcation have been predicted quantitatively. Furthermore, a preliminary three-dimensional simulation has shown the model's ability to deal with three-dimensional geometries. The method employed in our model does in no way obstruct the implementation of generalised Newtonian fluid behaviour and non-isothermal conditions; preliminary results are promising [19].

Further improvements of the model will include the implementation of faster and less memory-consuming solution methods, as the current solution method inhibits three-dimensional simulations of complex geometries. We also intend to test our simulation results against (non-isothermal) GAIM experiments. Finally, our aim is to include residual stress computations, since the reduction of residual stresses is one of the advantages of the GAIM process.

References

1 *Barton, K., Turng, L.*, in: ANTEC Proceedings, p. 421. Society of Plastics Engineers (1994)
2 *Polinski, A., Oehler, P., Stokes, V.:* Polym. Eng. Sci. 35, p. 877 (1995)
3 *Taylor, G.:* J. Fluid Mech. 10, p. 161 (1961)
4 *Polinski, A., Coyle, D.*, in: PPS 10th annual meeting, p. 219. Polymer Processing Society (1994)

5 *Costa, F., Thompson, W., Friedl, C.*, in: Simulation of materials processing: theory, methods and applications (Numiform *95)*, p. 1113, *Shen, S.-F., Dawson, P.* (Eds.). Balkema, Rotterdam (1995)
6 *Khayat, R., Derdouri, A., Herbert, L.:* J. Non-Newtonian Fluid Mech. 57, p. 253 (1995)
7 *Turng, L.:* Adv. Polym. Techn. 14, p. 1 (1995)
8 *Potente, H., Hansen, M.:* Int. Polym. Process. 8, p. 345 (1993)
9 *Halpern, D., Gaver III, D.:* J. Comp. Phys. 115, p. 366 (1994)
10 *Thompson, E.:* Int. J. Num. Meth. Fluids 6, p. 749 (1986)
11 *Chen, S., Cheng, N., Hsu, K.:* Int. J. Mech. Sci. 38, p. 335 (1996)
12 *Dussan V. E.:* Ann. Rev. Fluid Mech. 11, p. 371 (1979)
13 *Batchelor, G.*: An Introduction to Fluid Mechanics. Cambridge University Press, Cambridge (1967)
14 *Segal, A.:* SEPRAN manual. Ingenieursbureau SEPRA, Leidschendam 1996
15 *Cuvelier, C., Segal, A., van Steenhoven, A.:* Finite element methods and Navier-Stokes equations. Reidel, Dordrecht 1986
16 *Fortin, A., Béliveau, A., Demay, Y.*, in: Trends in Applications of Mathematics to Mechanics, *Marquez, M., Rodriguez, J.* (Eds.), Pitman (1995)
17 *Shahib, F.:* Ph.D. thesis, Stanford University, Stanford, Ca. (1988)
18 *Findeisen, H., Lanvers, A., Michaeli, W., Bender, K., Kirberg, K.:* Gasinjektionstechnik transparent gemacht. Videotape IKV Aachen 1991
19 *Zuidema, H.:* Master's thesis, Eindhoven University of Technology, WFW report 96.066 (1996)

Date received: September 1996
Date accepted: November 7, 1996